ELSEVIER

Contents lists available at ScienceDirect

Science Bulletin

journal homepage: www.elsevier.com/locate/scib



Short Communication

Hyperspectral imaging technique supports dynamic emission inventory of coal-fired power plants in China

Jinan Lin ^{a,b}, Chengzhi Xing ^{a,*}, Cheng Liu ^{a,b,c,d,*}, Wei Tan ^a, Wei Wang ^a, Peng Wu ^a, Chuan Lu ^a, Qihua Li ^e, Ting Liu ^f

- ^a Anhui Institute of Optics and Fine Mechanics, Hefei Institutes of Physical Science, Chinese Academy of Sciences, Hefei 230031, China
- b Department of Precision Machinery and Precision Instrumentation, University of Science and Technology of China, Hefei 230026, China
- ^c Centre for Excellence in Regional Atmospheric Environment, Institute of Urban Environment, Chinese Academy of Sciences, Xiamen 361021, China
- d Key Laboratory of Precision Scientific Instrumentation of Anhui Higher Education Institutes, University of Science and Technology of China, Hefei 230026, China
- ^e Institute of Physical Science and Information Technology, Anhui University, Hefei 230601, China
- ^fSchool of Earth and Space Sciences, University of Science and Technology of China, Hefei 230026, China

ARTICLE INFO

Article history:
Received 8 December 2022
Received in revised form 5 May 2023
Accepted 6 May 2023
Available online 22 May 2023

© 2023 Science China Press, Published by Elsevier B.V. and Science China Press, All rights reserved.

Since the industrial revolution until 2018, the extensive combustion of fossil fuels had increased carbon dioxide (CO_2) concentration in the atmosphere by 147%, reaching (407.8 \pm 0.1) ppm (1 ppm = 1 \times 10⁻⁶ L/L) [1]. The resulting greenhouse effect had triggered an increasing number of extreme climate disasters such as heat and cold waves [2–4]. The combustion of fossil fuels, particularly coal, typically produced high levels of polluting gases, such as nitric oxide (NO), nitrogen dioxide (NO₂), and sulfur dioxide (SO₂) [5], leading to an increase in the incidence and mortality rates of cardiopulmonary diseases, as well as a decline in urban visibility [6,7]. The emission inventories of coal-fired power plants, which were the primary source of these gases in cities, may vary depending on the power generation processes utilized [8]. Therefore, better observation of plant emissions was required.

Remote sensing methods have been widely used to monitor various air pollutants (including NO₂ and SO₂) [6,7]. One commonly used inversion method based on Lambert-Beer's law was differential optical absorption spectroscopy (DOAS), which was utilized to distinguish the spectral absorption characteristics of various trace gases [9]. Fourier transform infrared (FTIR) spectrometry, particularly EM27/SUN FTIR (EM27), was commonly used to collect direct solar radiation in the near-infrared spectral region to obtain column concentrations of CO₂, CH₄, and H₂O [10,11]. However, FTIR cannot image emissions because it can only retrieve greenhouse gases using direct sunlight [11]. Furthermore, researchers had employed remote sensing technology to monitor power plant emissions based on precise calculations of meteoro-

E-mail addresses: xingcz@aiofm.ac.cn (C. Xing), chliu81@ustc.edu.cn (C. Liu).

logical parameters, such as clouds [12–15]. Their findings revealed that the diffusion characteristics of NO_2 and CO_2 were similar over a broad range (R = 0.67), implying that the CO_2 emission characteristics of power plants can be characterized by NO_2 . In this study, we aimed to quantitatively image the exhaust gases (i.e., SO_2 and NO_2) emitted by power plants using joint observations of multi-axis-DOAS (MAX-DOAS) and EM27.

The coal-fired power plant investigated in this study was in located Hefei (31.91°N, 117.25°E), as shown in Fig. 1a. We conducted two observation campaigns on sunny days, one on November 30, 2020, and the other on June 2, 2022. The wind conditions during both campaigns were classified as Beaufort scale 3 in the northeast and southwest, with temperatures of approximately 279 and 306 K, and air quality index (AQI) values of 64 and 43, respectively. In the first campaign, a two-dimensional observation was performed using MAX-DOAS to directly obtain the image of NO₂ and SO₂ (Fig. 1b and File S1 online). In the second campaign, both EM27 and MAX-DOAS were operated in direct-sun observation mode. The top of the chimney's projection position was precalculated based on the solar zenith angle and solar azimuth angle, and the instrument location was immediately adjusted according to the plume's changes to ensure that the sun, plume, and instruments were always collinear in monitoring the concentration of plume components. Since water vapor emitted from coal-fired power plant chimneys can obstruct the sun and prevent the EM27 from obtaining spectra, the actual target area was located where water vapor dissipates (Fig. 1c).

The slant column densities (SCDs) of the trace gases observed by MAX-DOAS (File S1 online) were the path integral of the molecular concentration on the optical path. To eliminate the influence

^{*} Corresponding authors.

J. Lin et al. Science Bulletin 68 (2023) 1248–1251





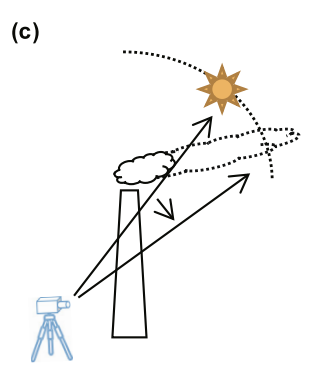


Fig. 1. (a) Aerial view of the campaign area obtained from Google Earth. The red circle indicated the location of the MAX-DOAS, and the blue circle represented the chimney, with a distance of 500 m between them. (b) The MAX-DOAS settings and weather condition during the campaign (see File S1 online for specific values of the 7 azimuth angles). (c) Schematic diagram of experimental setup for direct sun measurement.

of elevation angle on the integration path, we introduced the air mass factor (AMF). The vertical column density (VCD) of trace gases, corresponding to different elevation angles i, was calculated using

$$VCD(i) = SCD(i)/AMF(i).$$
 (1)

If there was no significant upwind emission source, their values were subtracted to obtain $VCD_{background-corrected}$ using

$$VCD_{\text{background-corrected}}(ij) = VCD(ij) - VCD(ij'),$$
 (2)

where j represented different azimuth angles and j' represented the upwind azimuth angle. High $VCD_{\rm background-corrected}$ values appeared within the plume area. Values outside the plume were considered to be due to fluctuations in the background values and were set to 0.

In this study, we assumed a circular cross-sectional shape for the plume. By knowing the distance D from the MAX-DOAS to the chimney (see Fig. 1a; D = 500 m), the plume radius r could be calculated based on a geometric relationship (Fig. S1 online). The calculated plume height h(i,j) at a certain elevation angle i and azimuth angle j could be calculated accordingly. The pathaveraged concentration $c_{i,j}$ can be calculated using

$$c(i,j) = k_1 \times M \times VCD(i,j)/(h(i,j) \times N_A), \tag{3}$$

where k_1 represented the unit conversion coefficient. When the unit of c(i,j) was mg m⁻³, k_1 equaled 1×10^7 (converted from g cm⁻² m⁻¹ to mg m⁻³). M represented the relative molecular mass of the target gas (g mol⁻¹), and N_A was the Avogadro constant (mol⁻¹).

Combined with wind field data, the emission fluxes F(j) of target gases can be further calculated using

$$F(j) = k_2 \times c(j) \times v \times \pi \times r^2 \times \sin\gamma, \tag{4}$$

where k_2 was another unit conversion coefficient. When F(j) was expressed as kg h⁻¹, k_2 equaled 3.6×10^{-3} (converted from mg s⁻¹ to kg h⁻¹). c(j) was the average concentration of the target trace gas observed at azimuth j. v represented the wind speed, and γ denoted the angle between the wind direction and the azimuth viewing angle.

We partitioned the CO_2 data into peak and non-peak sequences by applying a threshold equaled to the CO_2 background concentration plus 60% of the maximum concentration enhancement. The conversion coefficients k_{center} and $k_{boundary}$ (unit of both: molec cm⁻² cm² molec⁻¹) were computed at the center and boundary of the plume using Eqs. (5) and (6), respectively:

$$k_{\text{center}} = \frac{\overline{VCD_{\text{CO}_2}} - VCD_{\text{CO}_2, \text{background}}}{\overline{VCD_{\text{DS}}} - VCD_{\text{DS}, \text{background}}}, \quad VCD_{\text{CO}_2} > \text{threshold},$$
 (5)

$$k_{\text{boundary}} = \frac{\overline{VCD_{\text{CO}_2}} - VCD_{\text{CO}_2, \text{background}}}{\overline{VCD_{\text{DS}}} - VCD_{\text{DS}, \text{background}}}, \quad VCD_{\text{CO}_2} < \text{threshold}.$$
 (6)

The CO₂ VCD image of the plume was generated using

$$VCD_{CO_2 \text{ plume}} = \begin{cases} k_{\text{center}} VCD_{\text{plume}}, \text{centre}, \\ k_{\text{boundary}} VCD_{\text{plume}}, \text{boundary}. \end{cases}$$
 (7)

 \overline{VCD}_{CO_2} was the average value of the CO_2 VCDs that satisfied the conditions in Eqs. (5) and (6). \overline{VCD}_{DS} was the average NO_2 or SO_2 VCDs measured simultaneously with EM27 using the MAX-DOAS direct sun mode. The subscript "background" here referred to the average value during background observation. If the concentration of the polluted gas was lower than the detection limit of MAX-DOAS during the observation, the subscript "background" referred to the lowest value (for VCD_{DS}) when CO_2 was at the background level. VCD_{plume} was the NO_2 or SO_2 VCDs on the plume grid with the background concentration subtracted. The CO_2 emission fluxes could be calculated using Eq. (4).

Fig. 2a–f showed the average concentration of SO_2 and NO_2 in different light paths in three cases. The highest NO_2 concentration ((0.55 \pm 0.83) mg m⁻³) was observed in Case 1, while the highest SO_2 concentration ((3.67 \pm 2.80) mg m⁻³) was observed in Case 3. Both gases had low emissions in Case 2. Table S1 (online) displayed the average results for each case, indicating that the average fluxes of the both gases were maximum in Case 2 (NO_2 : (10.41 \pm 5.78) kg h⁻¹, SO_2 : (85.31 \pm 97.67) kg h⁻¹).

The time series of CO₂, NO₂, and SO₂ observed on June 2, 2022, were shown in Fig. S2 (online). Background observations were performed by the instruments prior to 08:24 (UTC), during which the average values of CO_2 and NO_2 VCDs were 6.02×10^{21} and 1.84×10^{15} molec cm⁻², respectively. The concentration of SO₂ was lower than the MAX-DOAS detection limit during this period. At \sim 8:24 (UTC), we first observed a high CO₂ VCD of 6.44 \times 10²¹ molec cm⁻² and simultaneously, the NO₂ and SO₂ VCDs increased to 1.31×10^{16} and 7.90×10^{16} molec cm⁻², respectively, which were significantly higher than the background values. During plume observation, we found strong correlations between the three components (Fig. S3 online), with the strongest correlation being between SO_2 and CO_2 VCDs (R = 0.90). The threshold CO_2 VCD was 6.54×10^{21} molec cm⁻², and only the MAX-DOAS averaged data with a time difference of less than 10 s with EM27 data were used. The CO₂ imaging results converted from SO₂ and NO₂ were shown in Fig. 2g-l. Among these three cases, the highest average CO_2 concentration was (36,498.16 ± 40,462.49) mg m⁻³ converted from SO₂ in Case 1, and the highest average CO₂ emission flux was (915,408.18 \pm 3,851,071.64) kg h⁻¹ in Case 2 (Table S2 online). It should be noted that the result converted from NO₂ was the same, although the values were slightly lower, which was $(35,069.90 \pm 54,957.60)$ mg m⁻³ in Case 1 and $(818,965.29 \pm 736,942.02)$ kg h⁻¹ in Case 2.

J. Lin et al. Science Bulletin 68 (2023) 1248–1251

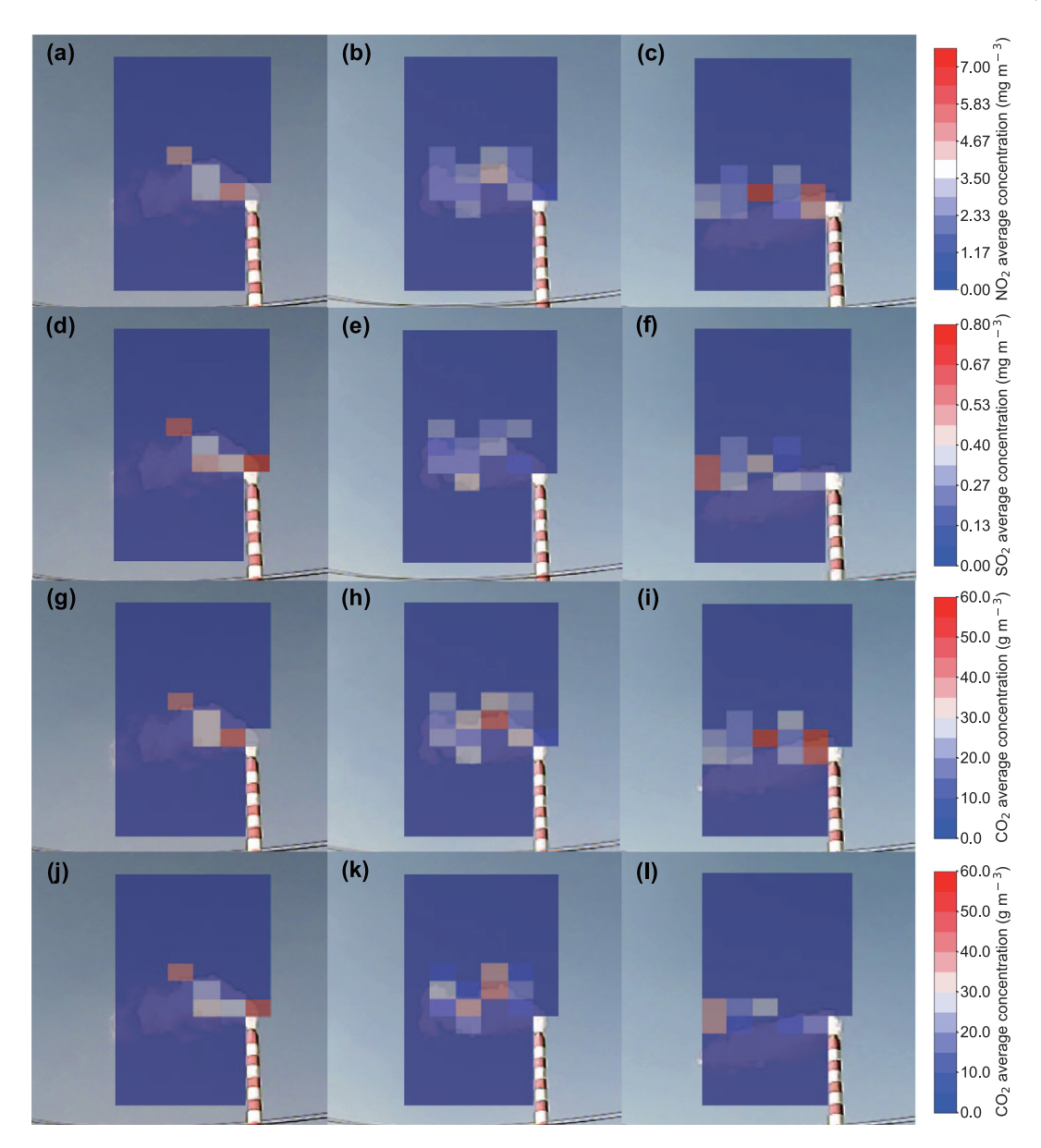


Fig. 2. Average concentration of SO₂ (a-c) and NO₂ (d-f) in different light paths in three cases: Case 1: UTC 2:47–3:08, Case 2: UTC 3:30–3:50, and Case 3: UTC 3:50–4:11. CO₂ imaging results were converted from SO₂ (g-i) and NO₂ (j-l).

According to the 2019 and 2020 annual enterprise environmental reports of Wanneng Hefei Power Generation Co., Ltd. (https://www. wenergy.cn/info.php?class_id=102104, last access date: March 2, 2021. Table S3 online), the power plant tested two units every quarter. The wintertime SO₂ and NO₂ concentrations were 12.0–22.7 and 1.0-1.7 mg m⁻³, respectively, which were generally 226.98%-804.38% and 81.82%-608.33% higher than those we measured. It should be noted that the SO₂ and NO₂ concentrations observed during sampling were only representative of their concentrations at the sampling site. The volume of the plume increased rapidly, resulting in a significant decrease in SO₂ and NO₂ concentrations after the exhaust gases were emitted from the chimney. Considering the annual operation time of these two power plant units (including the condition of these two units operating independently), the hourly averaged SO₂ and NO₂ emission fluxes of the power plant were 59.73 (=28.93 + 30.80) kg h^{-1} and 4.68 (=2.28 + 2.40) kg h^{-1} , respectively. The observed deviations of SO₂ and NO₂ in this study were -46.23%-42.82% and 0.37%-122.41%, respectively. Given that the maximum SO₂ and NO₂ concentrations were 44.58% and 66.50% higher than their minimum values during only one unit operation, respectively, the deviations of the SO_2 and NO_2 observation results were acceptable. Unfortunately, the environmental report of the power plant only provides total annual CO_2 emissions data for 2019, totaling 6,014,599,110 kg. Combining the operating time of the two units, we estimate the average CO_2 emissions flux of the single unit of the power plant to be 484,641.45 kg/h (969,282.90 kg/h when two units were working). Therefore, it indicated that the CO_2 imaging results were reliable and this technology can help improve the development of emission inventory.

The possible errors were primarily due to SCD retrievals, algorithm assumptions, and uncertainties in ancillary data. The uncertainties in the plume range, determined by the resolution of the elevation angles, introduced the maximum concentration errors. As a result, the errors of the final results were positively linear (Fig. S4 and File S1 online). It should be noted that the proportions of NO_2 , SO_2 , and CO_2 could be influenced by factors such as the output power, combustion conditions, and unit operation status, as well as other factors specific to coal-fired power plants.

To improve the understanding of the emission inventory of coal-fired power plants, we conducted joint observations near a

J. Lin et al. Science Bulletin 68 (2023) 1248–1251

power plant in Hefei using ground-based MAX-DOAS and EM27. This study found that SO₂, as a primary pollutant, was a better indicator of coal-fired power plant emissions and can be used to calibrate NO₂ and CO₂ emissions in areas where strict sulfur emission standards were enforced. Although this method required ideal meteorological conditions, it provided a remote and dynamic power plant emission inventory measurement scheme that can be easily applied to other scenarios (such as steel mills) to reduce air pollution and carbon emissions, and promote sustainable development. Moreover, this method had the potential to acquire extensive information on emissions, and was not limited to observations of the aforementioned gases.

Conflict of interest

The authors declare that they have no conflict of interest.

Acknowledgments

This work was supported by the National Key Research and Development Program of China (2022YFC3700100 2022YFC3704200), the National Natural Science Foundation of China (42207113), the Anhui Provincial Natural Science Foundation (2108085QD180), the Presidential Foundation of the Hefei Institutes of Physical Science, Chinese Academy Sciences (YZJJ2021QN06 and YZJJ2022QN05), the Strategic Priority Research Program of Chinese Academy of Sciences (XDA23020301), the Key Research and Development Project of Anhui Province (202104i07020002), the Major Projects of High Resolution Earth Observation Systems of National Science and Technology (05-Y30B01-9001-19/20-3), the Youth Innovation Promotion Association of Chinese Academy of Sciences (2021443), and the Young Talent Project of the Center for Excellence in Regional Atmospheric Environment, Chinese Academy of Sciences (CERAE202004). We would like to thank the groups of DOAS intelligent system (DOA-SIS), PROFFAST, SCIATRAN, and Weather Research and Forecasting/Chemistry (WRF-Chem) model.

Author contributions

Jinan Lin, Chengzhi Xing, and Cheng Liu designed and implemented the research, as well as prepared the paper. Jinan Lin, Chengzhi Xing, Wei Tan, Wei Wang, and Peng Wu carried out the MAX-DOAS and EM27 observations. Peng Wu contributed to the EM27 data retrieval. Chuan Lu contributed to the simulation of air mass factor. Qihua Li discussed the results. Ting Liu contributed to simulation of wind field. All co-authors commented on the paper and improved it.

Appendix A. Supplementary materials

Supplementary materials to this short communication can be found online at https://doi.org/10.1016/j.scib.2023.05.020.

References

- [1] World Meteorological Organization Atmospheric Environment Research Division, World Data Centre for Greenhouse Gases Japan Meteorological Agency. Isotopes confirm the dominant role of fossil fuel combustion in increasing levels of atmospheric carbon dioxide. WMO Greenh Gas Bull 2019:15. 6–7.
- [2] Camilo M, Daniele S, Erik CF, et al. Broad threat to humanity from cumulative climate hazards intensified by greenhouse gas emissions. Nat Clim Chang 2018:8:1062–71.
- [3] Song SY, Yeh SW, An SI, et al. Asymmetrical response of summer rainfall in East Asia to CO₂ forcing. Sci Bull 2021;67:213–22.
- [4] Zhou SJ, Huang P, Xie SP, et al. Varying contributions of fast and slow responses cause asymmetric tropical rainfall change between CO₂ ramp-up and rampdown. Sci Bull 2022;67:1702–11.

[5] Tian J, Ni HY, Han YM, et al. Primary PM_{2.5} and trace gas emissions from residential coal combustion: assessing semi-coke briquette for emission reduction in the Beijing-Tianjin-Hebei region, China. Atoms Environ 2018;191:378–86.

- [6] Xing CZ, Liu C, Wu H, et al. Ground-based vertical profile observations of atmospheric composition on the Tibetan Plateau (2017–2019). Earth Syst Sci Data 2021:13:4897–912.
- [7] Liu C, Xing CZ, Hu QH, et al. Stereoscopic hyperspectral remote sensing of the atmospheric environment: innovation and prospects. Earth-Sci Rev 2022;226:103958.
- [8] Tong D, Zhang Q, Liu F, et al. Current emissions and future mitigation pathways of coal-fired power plants in China from 2010 to 2030. Environ Sci Technol 2018;52:12905–14.
- [9] Hönninger G, von Friedeburg C, Platt U. Multi axis differential optical absorption spectroscopy (MAX-DOAS). Atmos Chem Phys 2004;4:231–54.
- [10] Gisi M, Hase F, Dohe S, et al. XCO₂-measurements with a tabletop FTS using solar absorption spectroscopy. Atmos Meas Tech 2012;5:2969–80.
- [11] Ohyama H, Shiomi K, Kikuchi N, et al. Quantifying CO₂ emissions from a thermal power plant based on CO₂ column measurements by portable Fourier transform spectrometers. Remote Sens Environ 2021;267:112714.
- [12] Fujinawa T, Kuze A, Suto H, et al. First concurrent observations of NO₂ and CO₂ from power plant plumes by airborne remote sensing. Geophys Res Lett 2021;48:e2021GL092685.
- [13] Rodica L, Manvendra KD, Bradley GH. Multiscale observations of CO₂, ¹³CO₂, and pollutants at Four Corners for emission verification and attribution. Proc Natl Acad Sci USA 2014;111:8386–91.
- [14] Shang HZ, Chen LF, Husi L, et al. Development of a daytime cloud and haze detection algorithm for Himawari-8 satellite measurements over central and eastern China. J Geophys Res: Atmos 2017;122:3528–43.
- [15] Husi L, Takashi MN, Takashi YN, et al. Ice cloud properties from Himawari-8/ AHI next-generation geostationary satellite: capability of the AHI to monitor the DC cloud generation process. IEEE Trans Geosci Remote Sens 2018;57:3229-39.



Jinan Lin is currently pursuing the Ph.D. degree at Anhui Institute of Optics and Fine Mechanics, Hefei Institutes of Physical Science, Chinese Academy of Sciences. His research interest includes the remote sensing quantitative observation of urban pollutants.



Chengzhi Xing received his Ph.D. degree in Environmental Science from the University of Science and Technology of China in 2020. Since 2020, he has been working at Anhui Institute of Optics and Fine Mechanics, Hefei Institutes of Physical Science, Chinese Academy of Sciences as an assistant researcher. His research interest includes hyperspectral remote sensing instruments, algorithms, and applications.



Cheng Liu received his Ph.D. degree in Environmental Physics from the University of Heidelberg in 2010. He was a postdoctoral researcher at Harvard University. Since 2015, he has been a professor with the University of Science and Technology of China. His research interest includes the remote sensing of air pollution gases and greenhouse gases from satellite and ground-based observations.